

Tightly-bound Cooper pair, quasiparticle kinks and clues on the pairing potential in a high T_c FeAs Superconductor

L. Wray,¹ D. Qian,¹ D. Hsieh,¹ Y. Xia,¹ L. Li,¹ J.G. Checkelsky,¹ A. Pasupathy,¹ K.K. Gomes,¹ A.V. Fedorov,² G.F. Chen,³ J.L. Luo,³ A. Yazdani,¹ N.P. Ong,¹ N.L. Wang,³ and M.Z. Hasan^{1,4},

¹Joseph Henry Laboratories of Physics, Department of Physics,
Princeton University, Princeton, NJ 08544, USA

²Lawrence Berkeley National Laboratory, Advanced Light Source, Berkeley, CA 94305, USA

³Beijing National Laboratory for Condensed Matter Physics,

Institute of Physics, Chinese Academy of Sciences, Beijing 100080, P.R. China

⁴Princeton Center for Complex Materials, Princeton University, Princeton, NJ 08544, USA

(Dated: 14th August, 2008)

We present a systematic photoemission study of the newly discovered high T_c superconductor class $(\text{Sr/Ba})_{1-x}\text{K}_x\text{Fe}_2\text{As}_2$. By utilizing a unique photon energy range and scattering geometry we resolve the details of the single particle dynamics of interacting electrons on the central Fermi surfaces of this series which shows overall strong coupling behavior ($2\phi_0/k_B T_c \approx 6$). Quasiparticle dispersion kinks are observed in a binding energy range of 15 to 50 meV which matches the magnetic excitation energy scales (parameterized by J_1, J_2). The size of the Cooper pair wavefunction is found to be less than 20 Å indicating a short in-plane scale uncharacteristic of a BCS-phonon scenario but suggestive of a phase factor in the global order parameter. The kink likely reflects contributions from the strongly frustrated fluctuating spin excitations and the soft phonons around 20-40 meV.

PACS numbers:

Recent discovery of superconductivity (T_c up to 55K) in iron-based layered compounds promises a new route to high temperature superconductivity [1, 2, 3, 4, 5]. This is quite remarkable in the view that the T_c in the pnictides is already larger than that observed in the single-layer cuprates. These superconductors belong to a comprehensive class of materials where many chemical substitutions are possible. Preliminary studies suggest that the superconducting state in these materials competes with a magnetically ordered state, and the proper description of the magnetically ordered state lies somewhat in between a strong correlation mediated interacting local moment magnetism and quasi-itineracy with a high degree of stripe-like frustration [5, 6, 7, 8, 9, 10, 11, 12, 13, 14, 15].

Angle-resolved photoemission spectroscopy (ARPES) is a powerful tool for investigating the microscopic electronic behavior of layered superconductors [16, 17, 18, 19]. In this work we report single-particle electronic structure results focusing on the details of the low-lying quasiparticle dynamics and the pair gap formation on very high quality ($T_c \approx 1\text{K}$ and surface-RMS $\approx 2\text{Å}$) single domain single crystal samples, which allow us to gain insight into connections between the superconductivity and magnetism not addressed by other spectroscopic work [17, 18, 19, 20]. Besides a magnitude-oscillating superconducting gap in crossing from the zone center to the zone corner, we observe that the quasiparticles are strongly scattered by collective processes around 15 to 50 meV binding energy range depending on the Fermi sur-

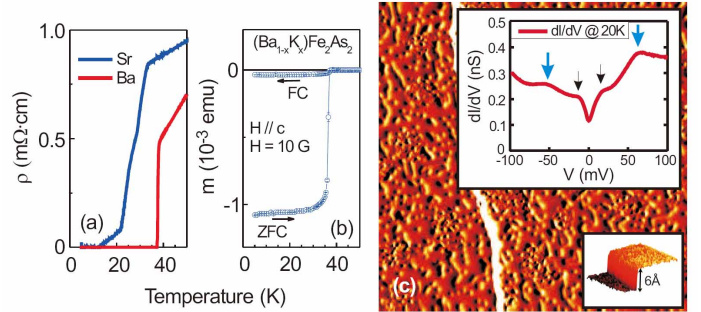


FIG. 1: Phase transition, magnetization profiles and surface quality. (a-b) Bulk T_c of crystalline $(\text{Ba},\text{K})\text{Fe}_2\text{As}_2$ and $(\text{Sr},\text{K})\text{Fe}_2\text{As}_2$ was determined based on the resistivity and magnetization profiles. $(\text{Ba},\text{K})\text{Fe}_2\text{As}_2$ samples exhibited $T_c = 37\text{K}$ and $T_c \approx 1\text{K}$ whereas $(\text{Sr},\text{K})\text{Fe}_2\text{As}_2$ samples exhibited a broad ($\approx 10\text{K}$) transition with a $T_c \approx 26\text{K}$. (c) Surface quality was studied by atomic-resolution STM measurements which exhibited a high degree of flatness and confirmed the suitability for spectroscopic measurements. The derivative of an STM image is shown which was taken on a $500\text{Å} \times 500\text{Å}$ patch. The inset shows low-temperature electronic gap on the order of 2 to 30 meV in superconducting samples. Sample batches with $T_c \approx 1\text{K}$ and smooth STM images were selected for UHV cleaves in our ARPES studies.

face sheet. Our high resolution and systematic quasiparticle data suggest that a Cooper pair in this superconductor is tightly bound ($\approx 4a_c$), reflecting a non-phononic character of the underlying pairing potential in light of retardation or screening effects. Overall results can be self-consistently interpreted in a phase-shifting order parameter scenario.

To whom correspondence should be addressed:
mzhasan@Princeton.EDU

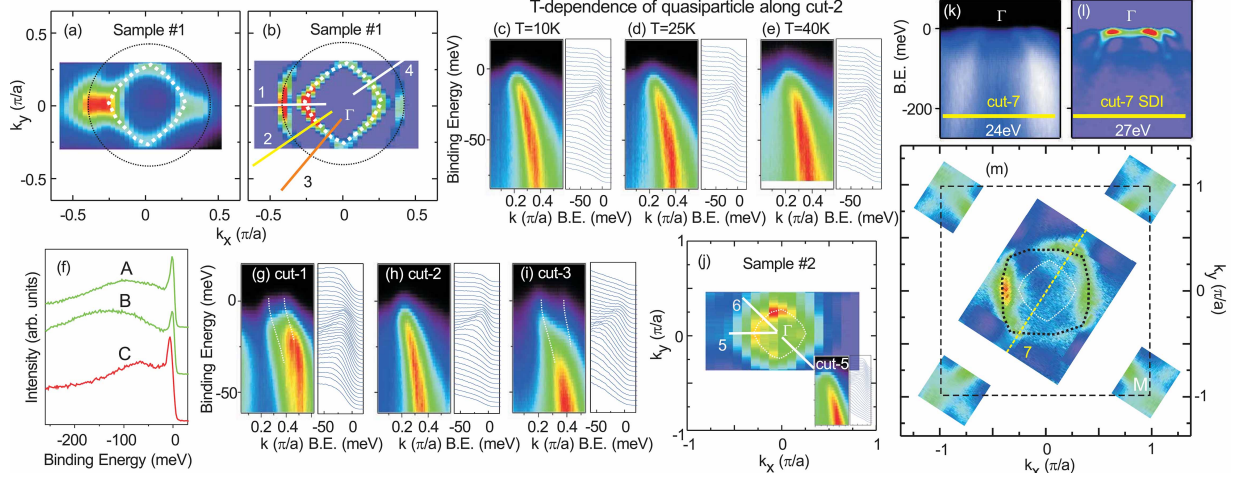


FIG. 2: Quasiparticle behavior on the Γ -point Fermi sheets in $(\text{Sr}=\text{Ba};\text{K})\text{Fe}_2\text{As}_2$. (a) Momentum distribution of quasiparticles within 15 meV of Fermi level in $(\text{Ba};\text{K})\text{Fe}_2\text{As}_2$. (b) Second-derivative image approximation of the Fermi surface topology around the Γ -point. (c-e) Quasiparticle dispersion along cut-2 and its temperature evolution. (f) High-resolution near-step binding energy scans shown for some selected k -space points near the $[1,0]$ and $[1,1]$ axes (A, B) on the outer FS surrounding the Γ -point, and on a separate FS close to the M-point (C). The k -space cut-2 strongly suppresses the outer FS and provides a clear spectroscopic look at the quasiparticle that forms the innermost FS. Because of the spectral clarity this quasiparticle can be studied in quantitative detail. (g-i) Quasiparticle intensity profiles along k -space cuts 1 to 3. The k -space cut-2 strongly suppresses the outer FS and provides a clear spectroscopic look at the quasiparticle that forms the innermost FS. Because of the spectral clarity this quasiparticle can be studied in quantitative detail. (j) Fermi surface image taken on $(\text{Sr};\text{K})\text{Fe}_2\text{As}_2$. (k,l) Wide k -range coarse-step scans are shown which was used for locating the Fermi crossings. (m) Electron distribution map, $n(k)$, within 15 meV of Fermi energy over the complete Brillouin Zone.

ARPES measurements were performed using 18 to 60 eV photons with better than 8 to 15 meV energy resolution respectively and overall angular resolution better than 1% of the Brillouin zone. Most of the data were taken at the Advanced Light Source beam line 12.0.1 and a limited data set was taken at SSRL beam line 5-4 for cross-checking, using a Scienta analyzer with chamber pressures lower than 5×10^{-11} torr. Linearly polarized photons were used for all the study. The angle between the \vec{E} -field of the incident light and the normal direction of the cleaved surface was set to about 45 degrees (at 12.0.1). Single crystalline samples of $\text{Ba}_{1-x}\text{K}_x\text{Fe}_2\text{As}_2$ ($T_c = 37\text{K}$) and $\text{Sr}_{1-x}\text{K}_x\text{Fe}_2\text{As}_2$ ($T_c = 26\text{K}$) were used for this systematic study. Cleaving the samples in situ at 15K resulted in shiny flat surfaces. Cleavage properties were characterized by atomic resolution STM measurements and the surface was found to be flat with an RMS deviation of 1Å (Fig. 1(c)). Rarely observed steps of size 6Å were seen on the otherwise flat surface. The utilization of a unique scattering geometry and specific photon energy range allowed us to suppress one of the FS sheets so that the other can be studied in full detail.

Quasiparticle behavior around the Γ -FS sheets is shown in Figure 2. Two square-like FS sheets were clearly resolved near the center of the BZ. An azimuthal variation of ARPES intensity around the FS pockets was observed. This variation is most pronounced while the data are taken at the particular photon-electron scattering geometry described above. A comparison of quasi-

particle dispersion measured along the various k -space cuts suggests that roughly along a cut 45-degrees to the $(\pi, 0)$ -line provides a clear spectroscopic look at the quasiparticle dispersion and lineshape behavior on the inner-FS. A bend in the dispersion (E vs. k) could be observed in the data which is not resolved in cut-1 or 3 due to the spectral overlap with the outer-FS. The measured quasiparticles in $\text{Sr}_{1-x}\text{K}_x\text{Fe}_2\text{As}_2$ were found to be broad and no bend could be resolved.

The temperature evolution of low-lying quasiparticles through the superconducting transition is shown in Figure 3. Quasiparticles gain spectral weight upon cooling below the transition temperature (37K). The low-temperature quasiparticle peak width is about 10 meV. The opening of the superconducting gap is best viewed upon symmetrization [21] of the near- E_F data and a gap magnitude of about 12 ± 2 meV is quite evident at low temperatures. This value is consistent with the average gap (< 15 meV, see Fig. 1(c)) we observe with STM on the same batch of samples. The observed gap value is found to be largest in the inner-most central FS (1 band), then decreases on the next FS (2 band) moving outward toward the M-point, and then increases again on the corner FS location. This oscillating gap structure is consistent with (but not a unique fit to) an order-parameter that takes the in-plane form of $\cos(k_x)\cos(k_y)$. The reduction of the gap value on the outer central FS is consistent with a $\cos k_x \cos k_y$ form. We caution that the ARPES data do not rule out the possibility of an out-of-plane (k_z)

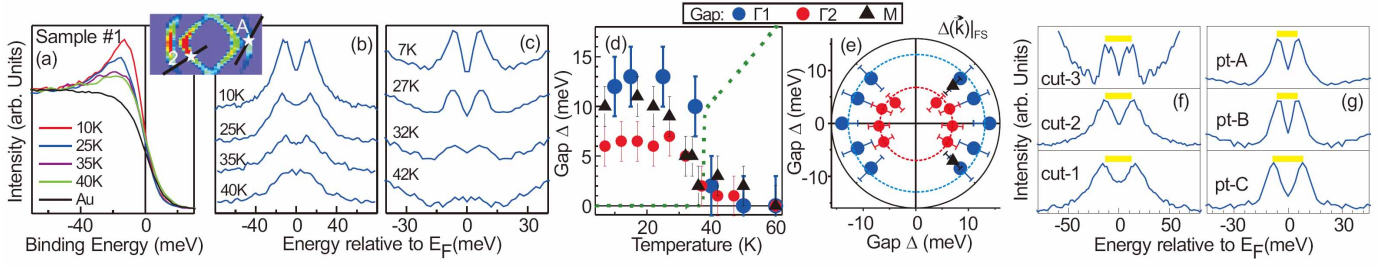


FIG. 3: Multi-gap pairing structure: (a) Temperature dependence of quasiparticles (cut-2) near the Fermi level through the superconducting transition. Below T_c samples exhibit coherence-peak-like behavior similar to what is observed in some cuprates. Temperature dependences of the gap at the k-space location of the innermost (1) FS (b) and the outer central (2) FS (c) are estimated by symmetrized spectral weight around the Fermi level. (d) The temperature dependences of the gaps measured at different FS locations (1-FS, blue; 2-FS, red; and near-M, black) are plotted along with the bulk resistivity curve (green). A fluctuation regime above T_c is observed. (e) The azimuthal k-dependence of gaps, $\Delta(k)_{FS}$, are shown for different FS sheet locations (1, 2, M). Selected EDCs are shown for the k-dependence of gaps on the inner (f) and outer Fermi surfaces (g). The cuts and pts refer to Fig. 2.

node in the order parameter. Existence of such a node may explain the in-gap T^3 behavior of NMR data [22].

A closer look at the quasiparticle dispersion behavior is presented in Figure 4. A bend in dispersion is evident in the momentum distribution curves (MDC) taken on a crossing near the 1-FS (cut-4). Each MDC could be fitted with a single Lorentzian over a wide binding energy range and, as in the raw data sets, the fitted peak positions trace a kink around 40–15 meV. This is further confirmed by examining the peak position of the real part of the self-energy which is also observed to be around 40–15 meV. Although it is less clear, the MDC width plotted as a function of the electron binding energy is found to exhibit a drop below 30 meV that is consistent with a kink at higher energy seen in the raw data. At temperatures above T_c the kink shifts to somewhat lower energies. As the temperature is raised further the MDCs are broadened making its identification or analytic extraction from our experimental data difficult and unreliable. In the MDC widths (Fig. 4(g)) an increase is observed at very low energies which was found to be unrelated to the existence of the kink but rather related to some residual signal from the tail of the quasiparticles on the outer FS. The STM data in Fig. 1(c) also exhibit a satellite structure around 40–50 meV loss-energy range (with respect to the quasiparticle peak position) roughly consistent with the observed ARPES kink. Assuming that the kink reflects coupling to some bosonic-like modes one can estimate the coupling strength: $\lambda_{eff}^0 \approx (0.7/0.45 - 1) \approx 0.6$. This coupling is about a factor of two to three larger than the electron-phonon coupling ($\lambda_{ph} \approx 0.2$) calculated for the Fe-As phonons near 20–40 meV [7]. A careful look at the outer central FS (2 band, cut-8) also reveals a kink around 18–5 meV. This kink is revealed when the band associated with the inner-FS sheet is suppressed by a choice of incident photon energy such as in the data taken near 18 eV. The observed kink energies seem to scale (40 meV and 18 meV) with the superconducting gap energies (12 meV and 6 meV) on the two

central Fermi surfaces (Fig. 4).

A strong-coupling kink phenomenology is observed in the electron dynamics of high T_c cuprates which occurs around 60–20 meV and is often attributed to phonons or magnetism or polarons with $\lambda_{eff}^0 \approx 1$ to 1.5 [16]. In cuprates the superexchange coupling is on the order of 130 meV, whereas the optical phonons are in the range of 40 to 80 meV overlapping with the kink. In the pnictides, although a T_c value of 37K is not outside the phonon-induced strong-coupling pairing regime, the vibrational modes of the FeAs plane are rather soft (≈ 35 meV) making electron-phonon interaction [7] an unlikely source of the majority part of the quasiparticle's self-energy beyond 40 meV, considering the observed coupling $\lambda_{eff}^0 \approx 0.6$ for the FeAs compounds here. The parent compounds of superconducting FeAs exhibit a robust SDW groundstate [5] due to a $\vec{Q} = (\pi, \pi)$ inter-band instability or due to the interaction of quasilocalized moments. The SDW short range order seems to survive well into the superconducting doping regime [23]. The doping evolution of the Fermi surface lacks robust nesting conditions for purely band magnetism to be operative at these high dopings and the relevant magnetism likely comes from the local exchange energy scales in a doping induced frustrated background. Therefore, quite naturally, strong spin fluctuations in the presence of electron-electron interaction are important contributors to the electron's self-energy and a natural candidate for the constituent of the kinks. In accounting for the parent SDW groundstates of these materials the known values of J_1 and J_2 are on the order of 20 to 50 meV [14, 15]. This is the energy range where we have observed the quasiparticle kinks (Fig. 4). In an itinerant picture, there exists a Stoner continuum whose energy scales are parameterized by J_1 and J_2 whereas in a local picture, J_1 and J_2 reflect Fe-Fe and Fe-As-Fe superexchange paths and the ground-state is a highly frustrated doped Heisenberg magnet [15]. The proper description of the experimentally observed magnetism in these systems lies somewhere in between.

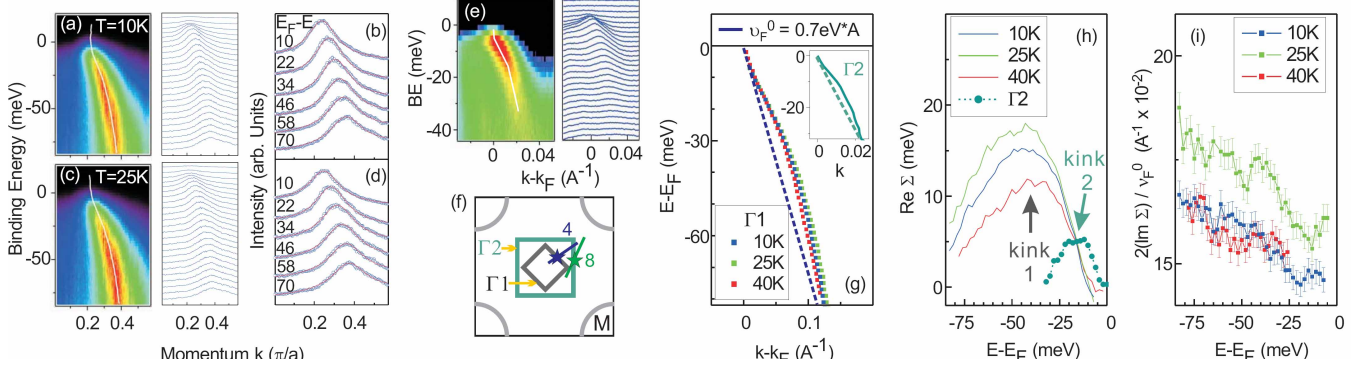


FIG. 4: D ispersio n kinks. (a),(c) Q uasiparticle band dispersion along cut-4 (k -space cut-4 is approximately along the Q_{AF} -vector of the undoped compound) and the corresponding MDCs at 10K and 25K. All the MDCs can be fitted by a single Lorentzian with linear background. (b),(d) The quasiparticle lineshapes are presented at selected energies (10–70 meV). (e) Band dispersion for the 2 quasiparticle along cut-8 shows a small kink near 18 meV. (f) Cuts 4 and 8 are labeled on a FS schematic. (g) By tracing the peak positions, quasiparticle band dispersion is plotted at $T=10K$, 25K and 40K. At all temperatures, the dispersion curve shows a "kink"-like feature at ~ 10 meV. The gray dashed line illustrates the "bare" band used for extracting the real part of the quasiparticle self-energy. The smaller kink at 18 meV on the 2 band is shown in the inset. (h) The real part of self energy is obtained by subtracting the gray dashed line from the experimental band dispersion. Peak position is used to define the "kink" position. (i) MDC width as a function of binding energy for quasiparticles on 1.

In the photoemission process removal of an electron from the crystal excites the modes the electron is coupled to, so the observed quasiparticle breaks the locally frustrated magnetic bonds associated with J_1 and J_2 which then contributes a characteristic energy scale in the electron's self-energy. Since these characteristic magnetic scales are quite large ($\sim 400K$) it is expected that the kink behavior in the electron's dispersion relation would survive above T_c consistent with our experimental observation. Despite the high signal-to-noise quality of our data, it is premature to draw an intimate connection between the kinks and the resonant spin mode (~ 15 meV) observed in neutron scattering [24].

High-resolution (Fig. 4) dispersion measurements further allow us to estimate the Fermi velocity of the normal state which is about 0.7 eV \AA . Using the observed superconducting gap (ARPES or STM data in Fig. 1) we can estimate the average size of the Cooper pair wavefunction: $\xi = \hbar v_F / \Delta$ by invoking the uncertainty relation [25]. Taking v_F (Fig. 4) $\sim 0.7 \pm 0.1 \text{ eV \AA}$ and a gap (Fig. 3) value of $\sim 12 \pm 2 \text{ meV}$, this gives $\xi \sim 20 \text{ \AA}$. This value is remarkably consistent with the high magnitude of H_{c2} ($\sim 70T$) [26] reported in these same materials. The ARPES based Cooper pair scale and unusually high H_{c2} clearly suggest that the Cooper pairs in this class of FeAs superconductors are tightly bound which is in contrast to the point-contact Andreev spectroscopy results on Sm-based FeAs superconductors exhibiting a conventional BCS ratio [27]. The agreement between ARPES, bulk H_{c2} and the bulk resistivity profile (Fig. 3(d)) provides further support for our identification of the superconducting gap and its bulk-representative value through a surface-sensitive measurement such as ARPES. This

also confirms that the ARPES observed gaps in superconducting materials [17, 18, 19] are not the SDW gaps as theoretically claimed by some authors. More importantly, such a small Cooper pair size scale ($\sim 4a_c$) is not known in any phonon-based BCS superconductor [28] but has only been observed in unconventional correlated superconductors. Our observed value is much smaller than that in the multiband s-wave BCS-phonon superconductors such as MgB₂ [28]. In fact a combination of small Cooper pair size and in-plane nodeless superconductivity is consistent with an unconventional $\cos(k_x)\cos(k_y)$ (in the unfolded BZ with one iron atom per unit cell)-type or $s_{x^2-y^2}$ or s-wave states [8, 9, 10, 11, 12, 13] since such an order parameter has a nearest-neighbor structure in real space and thus a reduction of the Coulomb interaction within the pair is naturally possible, so the electrons can come closer to each other leading to a short coherence scale. In cuprates pairing electrons come close to each other, and the short coherence length is achieved by introducing a node in the order parameter (d-wave) leading to a reduction of Coulomb interaction within the pair. This is often the only choice in a single band system such as the cuprates or the organics. In pnictides, multiband structure can accommodate a phase change without the need for introducing a "node" [29] on the Fermi surface, therefore an isotropic gap and short pairing scale can co-exist with a phase shifted order-parameter structure.

In summary, we have presented a single-particle study of high T_c superconductor class $(\text{Sr/Ba})_{1-x}\text{K}_x\text{Fe}_2\text{As}_2$. Our systematic ARPES data suggest an unusually small dimension of the Cooper pair, complex kink phenomena and an oscillating gap function all of which collectively point to an unconventional pairing potential. We have

presented arguments that in the presence of Coulomb interaction and magnetism, the observed short pairing scale and a nearly-isotropic in-plane gap can be self-

consistently realized if the order parameter contains a phase factor. Our results thus provide important clues to a novel route to high temperature superconductivity.

-
- [1] Y. Kamihara et al., *J. Am. Chem. Soc.* **130**, 3296 (2008).
 - [2] Z. A. Ren et al., *Chin. Phys. Lett.* **25**, 2215 (2008).
 - [3] G.-F. Chen et al., *Phys. Rev. Lett.* **100**, 247002 (2008).
 - [4] X. H. Chen et al., *Nature* **453**, 761 (2008).
 - [5] C. de la Cruz et al., *Nature* **453**, 899 (2008).
 - [6] D. J. Singh & M. Du, *Phys. Rev. Lett.* **100**, 237003 (2008).
 - [7] L. Boeri et al., *Phys. Rev. Lett.* **101**, 024603 (2008).
 - [8] I. I. Mazin et al., arXiv:0803.2740v3 (2008).
 - [9] K. Kuroki et al., arXiv:0803.3325v2 (2008).
 - [10] Z.-J. Yao, J.-X. Li, Z. D. Wang arXiv:0804.4166v2 (2008).
 - [11] K. Seo, B. A. Bernevig & J. Hu arXiv:0805.2958 (2008).
 - [12] M. Korshunov and I. Eremin arXiv:0804.1793v1 (2008).
 - [13] V. Cvetkovic and Z. Tesanovic arXiv:0804.4678v3 (2008).
 - [14] T. Yildirim, *Phys. Rev. Lett.* **101**, 057010 (2008).
 - [15] F. Ma, Z.-Y. Lu, and T. Xiang, arXiv:0806.3526 (2008).
 - [16] A. Damascelli et al., *Rev. Mod. Phys.*, **75**, 473 (2003);
J. C. Campuzano et al., *Photoemission in the high T_c superconductors*, v-2, p167265. Springer, Berlin, (2004);
P. D. Johnson et al., *Phys. Rev. Lett.* **87**, 177007 (2001).
 - [17] L. Zhao et al., arXiv:0807.0398 (2008).
 - [18] H. Ding et al., arXiv:0807.0419v1 (2008).
 - [19] C. Liu et al., arXiv:0806.3453v1 (2008).
 - [20] D.-H. Lu et al., arXiv:0807.2009v1 (2008).
 - [21] M. R. Norman et al., *Phys. Rev. B* **57**, R11093 (1998).
 - [22] H.-J. Graf et al., arXiv:0805.2595 (2008).
 - [23] H. Chen et al., arXiv:0807.3950v1 (2008).
 - [24] A. D. Christianson et al., arXiv:0807.3932v1 (2008).
 - [25] M. Tinkham "Introduction to Superconductivity", 2nd Ed., McGraw-Hill, New York (1996).
 - [26] H. Q. Yuan et al., arXiv:0807.3137v2 (2008).
 - [27] T. Y. Chen et al., *Nature* **453**, 1224 (2008).
 - [28] E. W. Carlson et al., in *The Physics of Conventional and Unconventional Superconductors*, edited by K. Bennemann and J. Ketterson (Springer-Verlag, Berlin, 2002).
 - [29] The $\cos \theta \cos \phi$ gap does have a node in it but the node does not intersect the Fermi surface as we measure here (Figure 3). However, it is clear that nearest or next nearest neighbour structure of the gap lowers the kinetic energy as opposed to a constant on-site s-wave gap.
 - [30] We thank B. A. Bernevig for helpful comments on the manuscript.

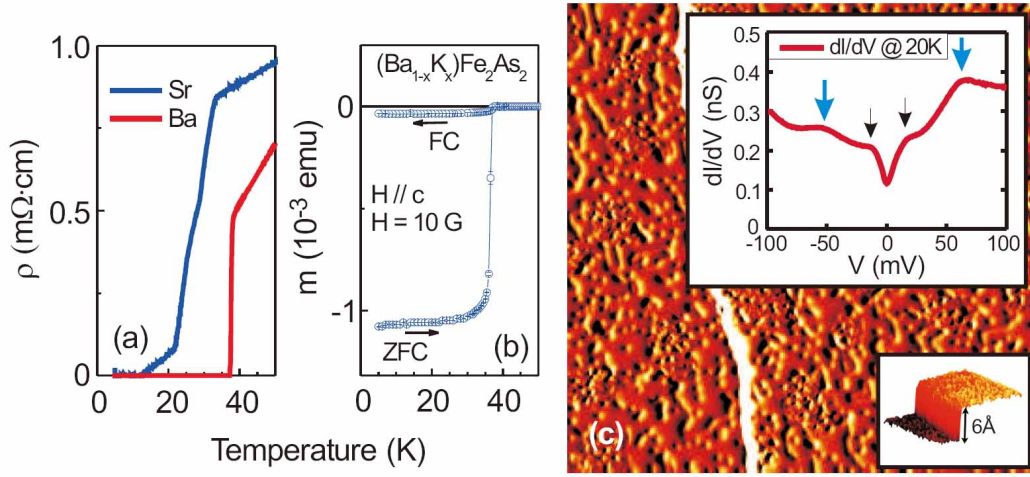


FIG. 5: Enlarged V iew of F igure 1.

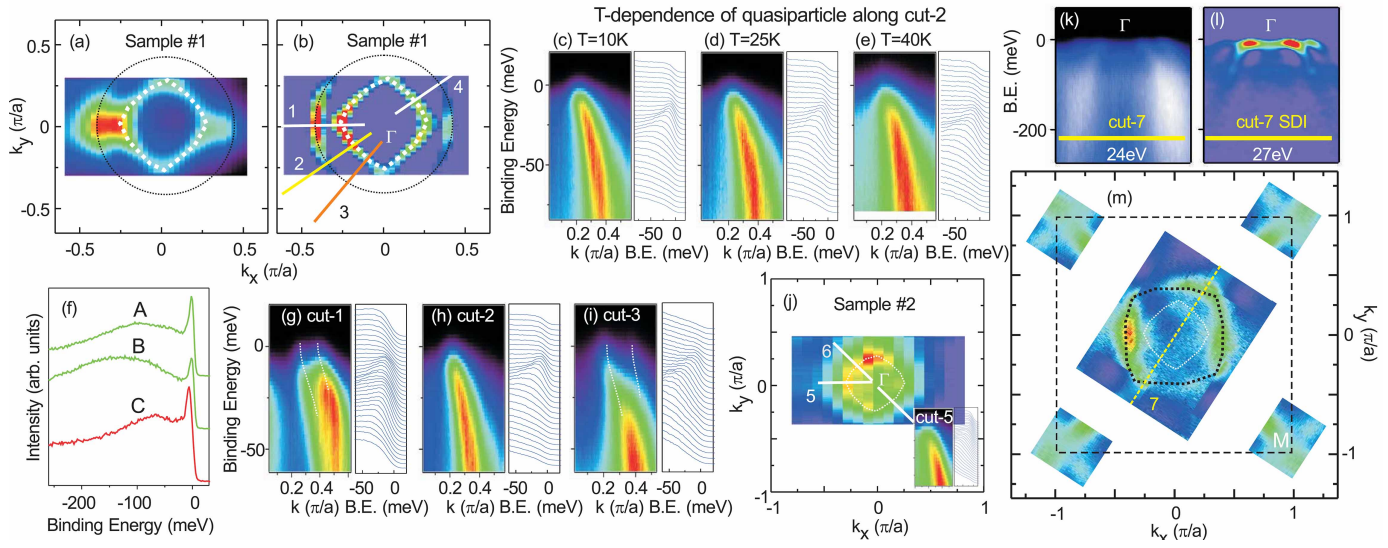


FIG. 6: Enlarged V iew of F igure 2.

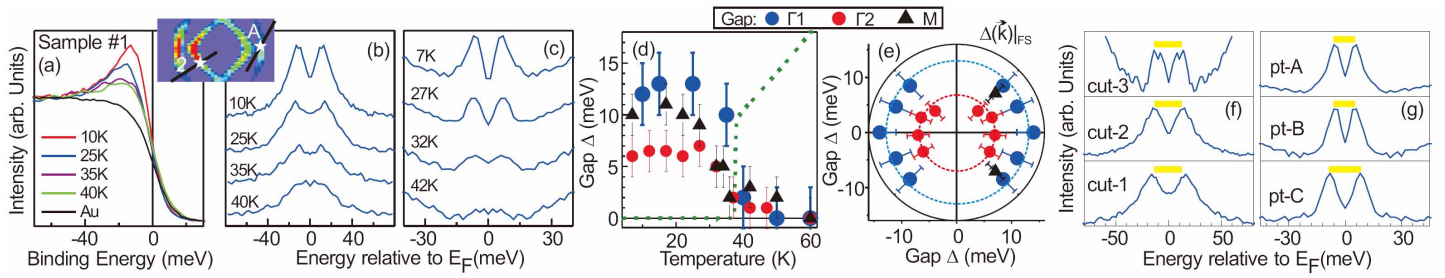


FIG. 7: Enlarged V iew of F igure 3

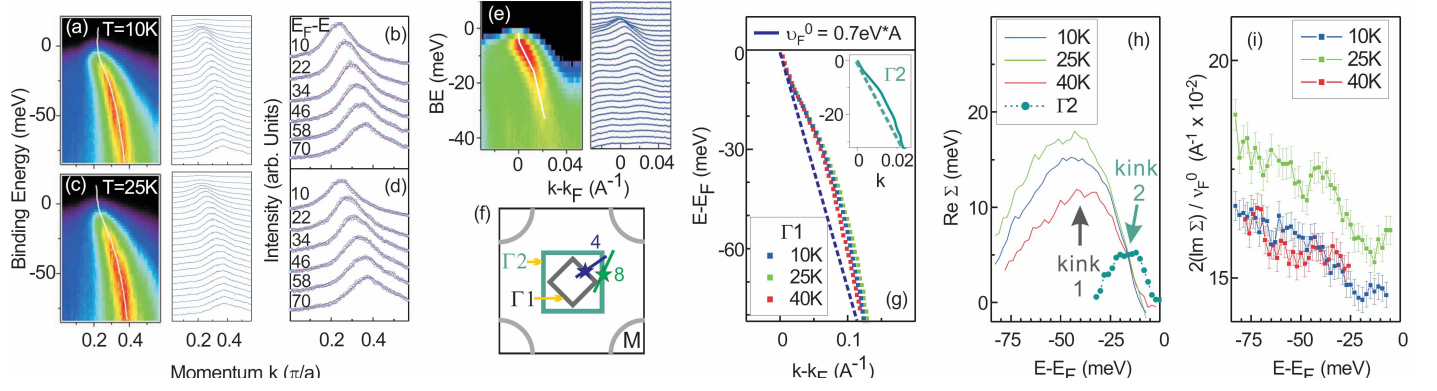


FIG. 8: Enlarged View of Figure 4.